ICARUS **122,** 366–382 (1996)
ARTICLE NO. 0130

Optical Effects of Regolith Processes on S-Asteroids as Simulated by Laser Shots on Ordinary Chondrite and Other Mafic Materials

L. V. MOROZ, A. V. FISENKO, AND L. F. SEMJONOVA

Vernadsky Institute of Geochemistry and Analytical Chemistry, Russian Academy of Sciences, Kosygin St. 19, 117975, Moscow, Russia
E-mail: abasilevsky@glas.apc.org

C. M. PIETERS

Brown University, Box 1846, Providence, Rhode Island 02912

AND

N. N. KOROTAEVA

Geological Department, Moscow State University, Vorobievy Gory, Moscow, Russia

Received February 16, 1995; revised November 22, 1995

Laboratory results from a simulation of possible optical effects of impact melting and repeated crystallization on asteroidal surfaces are presented. Quick melting and crystallization of surface materials were simulated by impulse laser treatment of powdered materials in vacuum. The mafic materials used in this study were: ordinary chondrite (OC) Elenovka *L*5, carbonaceous chondrite Allende CV3, terrestrial olivine, clinopyroxene, and olivine–clinopyroxene mixture 1 : 1. The reflectance spectra of powdered samples before and after laser treatment were recorded in the range 0.3–25 μm. The laboratory laser alteration produced a reduction in overall reflectance and spectral contrast, a noticeable increase in spectral slope, the shifts in the wavelength positions of absorption band centers, and a decrease in band area ratio. The continuum slope of the ordinary chondrite Elenovka after laser treatment is comparable to that of S-type asteroids. Laser impulse alteration raises the spectrally derived olivine/orthopyroxene ratio of Elenovka from 2.8 to 5.4. This value is far outside the OC range, but falls within the olivine/orthopyroxene range for S-asteroids. The results suggest that quick melting and subsequent crystallization can enhance the spectral similarity between S-asteroids and ordinary chondrites. © 1996 Academic Press, Inc.

1. INTRODUCTION

The longest controversy in asteroid science concerns the mineral composition of S-type asteroids and possible genetic links between these asteroids and the ordinary chondrites. Ordinary chondrites (OCs) are known to make up ~80% of observed meteorite falls, but so far very few asteroid spectral analogs have been identified for these meteorites.

The S-asteroids are widespread in the inner belt and appear to consist mostly of olivine, orthopyroxene, and metal. They resemble OCs spectrally but are characterized by steep red continua unlike those of the OCs, and their spectrally derived mineralogies are far outside the OC range (Gaffey *et al.* 1993a). Moreover, the character of the rotational spectral variations of surfaces of two large S-asteroids, 8 Flora and 15 Eunomia, appear to be inconsistent with the primitive undifferentiated OC composition (Gaffey 1984, Gaffey and Ostro 1987). Consequently, the majority of investigators are inclined to interpret S-type asteroids as composed of various differentiated assemblages which are the products of melting in the deep interiors of asteroid parent bodies. These materials are similar to stony-iron meteorites and some achondrites (Gaffey 1993a, Hiroi *et al.* 1993a).

Thus, the source of ordinary chondrites remains unclear. On the basis of some spectral resemblance between the shocked (black) OCs and C-type asteroids, Britt and Pieters (1987) proposed that OC parent bodies are "masked" among the C-asteroid population, but such an idea is not consistent with the results of photopolarimetric studies (e.g., Shkuratov 1994). Bell *et al.* (1989) suggested that OC parent bodies can be found among the small primordial main belt S-objects, which have not undergone any internal differentiation unlike larger S-asteroids and their frag-

0019-1035/96 $18.00
Copyright © 1996 by Academic Press, Inc.
All rights of reproduction in any form reserved.

TABLE I
Microprobe Analyses of Unaltered Minerals and Various Constituents of Altered Materials

	Unaltered minerals		Altered olivine			Altered pyroxene		Altered olivine–clinopyroxene mixture			
	Olivine	Pyroxene	Bulk "melt"	Ol crystals in melt	Mesostasis	Glass	Crystallized pyroxene	Bulk "melt"	Ol crystals in melt	Mesostasis	Unfused Ol clasts
SiO_2	39.87	53.21	41.45	41.13	48.50	50.52	54.43	45.18	41.70	50.12	40.11
TiO_2	0.01	0.55	0.03	0.01	0.13	0.56	0.39	0.29	0.02	0.55	0.01
Al_2O_3	0.02	2.64	0.47	0.05	3.72	5.41	2.22	3.36	0.06	5.00	0.02
Cr_2O_3	0.03	0.16	0.07	0.02	0.06	0.11	0.34	0.09	0.05	0.04	0.03
FeO	9.85	5.48	9.72	4.49	35.65	6.50	2.99	7.21	4.49	9.20	9.28
MnO	0.15	0.17	0.12	0.06	0.42	0.16	0.07	0.13	0.14	0.14	0.14
MgO	48.46	15.66	47.44	53.42	9.19	17.81	19.42	32.29	52.81	16.02	49.31
CaO	0.05	22.20	0.27	0.03	1.53	19.11	19.86	10.98	0.88	19.36	0.10
NiO	0.36	0.06	0.26	0.20	0.11	0.14	0.06	0.17	0.18	0.02	0.40
Na_2O	0.07	0.46	0.16	0.13	0.54	0.44	0.21	0.27	0.06	0.15	0.08
K_2O	0.01	0.03	0.02	0.01	0.07	0.01	0.01	0.03	0.01	0.01	0.00
Total	98.88	100.62	100.01	99.55	99.92	100.77	100.00	100.00	100.39	100.61	99.48
Fo	89.8			95.5					95.5		90.5
Fa	10.2			4.5					4.5		9.5
Wo		46.0					44.5				
En		45.1					47.0				
Fs		8.9					8.5				

ments. However, observations of Binzel *et al.* (1993) show that only one of 50 small main belt S-asteroids observed has a spectral resemblance with ordinary chondrites.

It was also proposed that the spectral mismatch between S-type asteroids and OC meteorites results from some "space weathering" process which alters the optical properties of the uppermost regolith (Feierberg *et al.* 1982, McFadden 1983, Pieters 1984). However, the spectral studies of shocked (black) OCs (Britt and Pieters 1990, Keil *et al.* 1992), gas-rich OCs (Bell and Keil 1988, Britt and Pieters 1991), melted OCs (Clark *et al.* 1992), and synthetic metal-rich regoliths derived from OCs (Gaffey 1984) demonstrate that such altered OC materials darken, but do not redden sufficiently to match the S-type spectral characteristics.

Nevertheless, plausible regolith processes remain which could explain the spectral reddening of S-asteroid surfaces. Studies of lunar regolith fractions indicate that the red slopes of lunar soil spectra appear to result from the solar wind induced reduction of silicate iron (Pieters *et al.* 1993, Starukhina *et al.* 1994, Allen *et al.* 1993). The impact-induced process of vaporization and recondensation causes both the reduction of silicate iron and some other chemical effects (Cassidy and Hapke 1975, Yakovlev *et al.* 1992, Keller and McKay 1992, Dikov *et al.* 1994). The laboratory simulations of impact-induced vaporization and redeposition demonstrate that impact processes may result in various reduction–oxidation reactions, for example, oxidation of Fe, Cr, Al, or reduction of Fe, Si, P, Al. Laboratory experiments show that the same elements can be reduced or oxidized depending on the experimental conditions (temperature, pressure) and the composition of both impactor and target (Yakovlev *et al.* 1992). The conditions which are necessary for specific redox reactions in the impact melt, as well as in the vapor, are poorly understood. Experiments by Danielson and Jones (1995) show that the heating of olivine grains in H_2 or Ar atmosphere to 1200–1500°C result in the reduction of ferrous iron and the formation of submicroscopic metallic iron (SMFe). The fact that the reduction of Fe was observed in Ar atmosphere indicates that the presence of H_2 is not necessary for this reaction (Danielson and Jones 1995). The impact-induced reduction of silicate iron, which can occur both in the impact melt and in the impact-generated vapor, appears to be an optically important effect. Keller and McKay (1992) have detected vapor deposited coatings on lunar soil particles. These coatings are enriched in Si and Fe, much of the later being SMFe. Theoretical models calculated by Hapke (1993) demonstrate that SMFe distributed throughout the glass and also coating the crystalline grains can account for the optical properties of lunar soils. The SMFe reduces the albedo and spectral constrast, reddening the spectrum.

The present study will further investigate the possible role of space weathering in the alteration of optical surfaces of atmosphereless bodies and particularly of possible S-asteroid material analogs. We attempt to evaluate the possible optical effects of rapid melting and subsequent crystallization of surface materials, which may be caused by meteorite bombardment, for example, by micrometeoroid impacts. The goal of this work is not to evaluate the plausibility of the formation of impact melt on asteroid surfaces. Rather, we try to estimate the possible optical effects of impact melt formation and repeated crystallization, assuming these processes may produce optically important changes on asteroid surfaces. We did not try to simulate

TABLE I—*Continued*

	Elenovka					Allende		
	Bulk "melt"	Ol crystals in melt	Mesostasis	Unfused Ol clasts	Unfused Px clasts	Bulk "melt"	Ol crystals in melt	Mesostasis
SiO_2	45.39	41.43	52.40	38.93	54.70	34.53	38.63	31.20
TiO_2	0.10	0.01	0.35	0.01	0.21	0.16	0.02	0.44
Al_2O_3	2.57	0.06	5.55	0.03	0.02	3.70	0.36	12.30
Cr_2O_3	0.52	0.23	0.65	0.02	0.02	0.56	0.35	0.49
FeO	18.42	10.54	24.65	21.36	15.17	29.77	17.09	38.61
MnO	0.51	0.19	0.66	0.48	0.50	0.20	0.12	0.26
MgO	30.11	48.10	8.08	39.00	28.09	27.22	42.87	2.75
CaO	1.67	0.14	5.52	0.03	0.79	2.98	0.41	12.76
NiO	0.05	0.02	0.12	0.02	0.00	0.08	0.23	0.08
Na_2O	0.64	0.08	0.75	0.11	0.32	0.31	0.24	0.21
K_2O	0.05	0.01	0.06	0.00	0.04	0.01	0.01	0.05
SO_2	n.d.	n.d.	1.20	n.d.	0.14	0.47	0.11	0.85
Total	100.03	100.81	99.99	99.99	100.01	99.99	100.44	100.00
Fo		89		76.5			81.7	
Fa		11		23.5			18.3	
Wo					1.5			
En					75.6			
Fs					22.9			

meteorite impacts by using comparable experimental conditions (to use comparable energies and temperatures or to generate shock waves), nor do we claim that laser shots are good simulants of micrometeoroid bombardment. We simulated only one of the possible aspects of impact processes—namely, *quick* (first seconds) melting and cooling of materials. Unlike the earlier work of Clark *et al.* (1992) who used a fusion furnace, we used laser irradiation to simulate rapid melting and cooling of the samples.

2. EXPERIMENTAL PROCEDURE

Several different materials were selected for this study: ordinary chondrite Elenovka *L5*, carbonaceous chondrite Allende CV3, terrestrial olivine, clinopyroxene, and olivine–clinopyroxene mixture 1:1. Microprobe analyses of olivine and orthopyroxene are presented in Table I. Samples were ground and sieved to a particle size <75 μm ("unaltered samples"). To evaluate possible spectral effects of quick melting and subsequent crystallization the powdered specimens were treated by laser irradiation under vacuum at 5×10^{-5} mm Hg using the Vernadsky Institute laser facility LTI-501-01. A solid-state ND-YAG multiple-pulse laser with impulse frequency 30–40 KHz was used for the experiment. The wavelength of laser irradiation was 1.06 μm and the diameter of the focused laser beam was $\sim$100 μm. Pulse duration was 0.5–1 μsec, and laser power was about 1.2 KW. The powdered samples were placed in a stainless steel holder. The thickness of the powder layer on the holder was 1 mm. The laser power was insufficient to penetrate such a thick layer of powder, so the holder was not caught up during the experiment and altered materials were not contaminated. The sample holder was rotated at a velocity of two revolutions per minute during the experiment, and could be shifted relative to the laser beam in the radial direction. The use of a turbomolecular pump TMN-500 in the vacuum system allowed avoidance of the contamination of the samples by oil vapor.

As a result of laser treatment, some particles were fused and stuck together into "glassy" aggregates described below. After the laser alteration the powders were repeatedly sieved. The coarser size fraction (>75 μm) completely consisted of altered glassy aggregates. These fused and repeatedly crystallized materials are called "altered samples" in the present paper. The finer separates include both unaltered particles and part of altered fused and crystallized aggregates, which do not exceed the size of 75 μm. These separates, containing both unaltered and altered particles are called "partly altered samples" in this paper. The coarser altered samples were reground to a particle size of <75 μm before spectral measurements. It should be noted that altered aggregates still contain from 8 to 36% of unaltered clasts, which were unfused or stuck to the cooling melted particles (Table II).

Chemical compositions of various components of the samples were determined at the Moscow State University Camebax SX 50 microprobe facility operated at 15 KV and 30 nA, and SEM (CamScan 4 DV) with the energy dispersive attachment Link AN-10000 operated at 15 KV and 1.2 nA.

After the laser experiment the reflectance spectra of the unaltered, partly altered, and altered samples were measured. Bidirectional reflectance spectra in the range 0.3–2.7 μm at a viewing geometry $i = 30°$, $e = 0°$ were recorded with the NASA RELAB bidirectional spectrom-

TABLE II
Modal Analyses of Various Constituents of Altered Materials (Vol%)

	Ol	Px	mix.[a]	El.[b]	All.[c]
Unfused clasts[d]					
olivine	36	—	8	14	11
pyroxene	—	3	—	4	—
"Melt" (including quench crystallized materials)[d]	58	97	92	75	84
Metal and troilite[d]	—	—	—	7	5
	100	100	100	100	100
"Melt"					
mesostasis	14	—	46	39	38
olivine crystals	86	—	54	61	62
	100	100	100	100	100
Vesicles	6	42	14	10	21

[a] mix—olivine/clinopyroxene mixture.
[b] El.—Elenovka (*L*5).
[c] All.—Allende (CV3).
[d] Vesicles are subtracted.

eter at Brown University. All spectra were measured relative to halon, a near perfect diffuse reflector in the 0.3–2.7 μm region (Weidner and Hsia 1981).

Spectra from 1.27 to 25 μm were acquired with a Nicolet 740 FTIR spectrometer (Brown University) using a biconical reflectance attachment. The spectra were measured relative to a rough gold standard in an H_2O and CO_2 purged environment. The infrared data were scaled to the spectra which were recorded with the RELAB bidirectional spectrometer under ambient conditions using halon as a standard. At present mid-infrared spectra are not useful for comparisons with telescopic data since no data on asteroids exist in that wavelength region. Therefore, most of the mid-infrared data are not presented in this paper except for the most important results for discussion purposes.

The most abundant components of the materials used in this study are olivines (ol) and/or pyroxenes (px). Besides the pure olivine samples and the olivine/pyroxene mixture, olivine is major constituent of Elenovka and Allende meteorites. Reflectance spectra of olivines exhibit a complex absorption band near 1 μm (band I) which is composed of three overlapping bands attributable to crystal field transitions in ferrous iron (Burns 1970a).

Pyroxenes considered in this paper are of two types. (i) Low calcium content pyroxene–orthopyroxene (Fs 19–23) is one of the major components of Elenovka meteorite (Baryshnikova and Lavrukhina 1979). Orthopyroxenes and low calcium content clinopyroxenes exhibit two major absorption bands centered near ~0.9–0.94 μm (band I) and ~1.8–2.1 μm (band II) also due to Fe^{2+} crystal field transitions (Burns 1970b). (ii) The high calcium content clinopyroxene used in this study also shows two major absorptions, but they are centered near 1.05 μm (band I) and 2.3 μm (band II). The wavelength positions of the bands are typical of clinopyroxenes the compositions of which are close to those of diopsides (Cloutis and Gaffey (1991). This high calcium clinopyroxene belongs to spectral type B of Cloutis and Gaffey (1991), which is characterized by two major absorption bands centered near ~0.96–1.05 μm (band I) and ~2.1–2.4 μm (band II). We occasionally used terrestrial high calcium clinopyroxene (cpx) for laser experiments, even though it seems more reasonable to use orthopyroxene, since most pyroxenes in meteorites (and Elenovka in particular) have low calcium contents. Nevertheless, we include the results on cpx and the ol/cpx mixture in the present paper. We consider these results to be important ones, since they confirm one of the main conclusions of our work, concerning the "disappearance" of pyroxene absorption bands in the spectra of altered ol, px-bearing materials (see below).

Straight line continuum removal has been performed in some cases to isolate specific absorption bands (band I, band II, and complex features between 4.5 and 7 μm). Band centers were calculated by 2nd or 3rd order polynomial fitting to ~10 data points on either side of the visually determined center after dividing out the linear continuum. Spectral slopes for Elenovka samples were calculated from the fitted continuum across band I as the rise in reflectance divided by the change in wavelength (Clark and Roush 1984). Band depths are defined as

$$D = (R_c - R_b)/R_c,$$

where R_c is reflectance of the continuum at the band center, R_b is reflectance of the sample at the band center, and D is the band depth (Clark and Roush 1984). The ratios of the areas of band II to band I have been calculated for Elenovka following the procedure outlined by Cloutis *et al.* (1986). The modified Gaussian model analysis (Sunshine *et al.* 1990) was applied to deconvolve VNIR (visual–near-infrared) reflectance spectra of the pure olivine series.

3. MINERALOGY AND PETROGRAPHY OF ALTERED MATERIALS

The laser treatment resulted in the formation of glassy droplets approaching 500 μm in diameter. Sometimes they stick together forming aggregates which resemble a bunch of grapes (Allende, pure cpx). Sometimes they form irregular aggregates without clear boundaries between single droplets (pure ol, ol/cpx mixture). Elenovka altered sam-

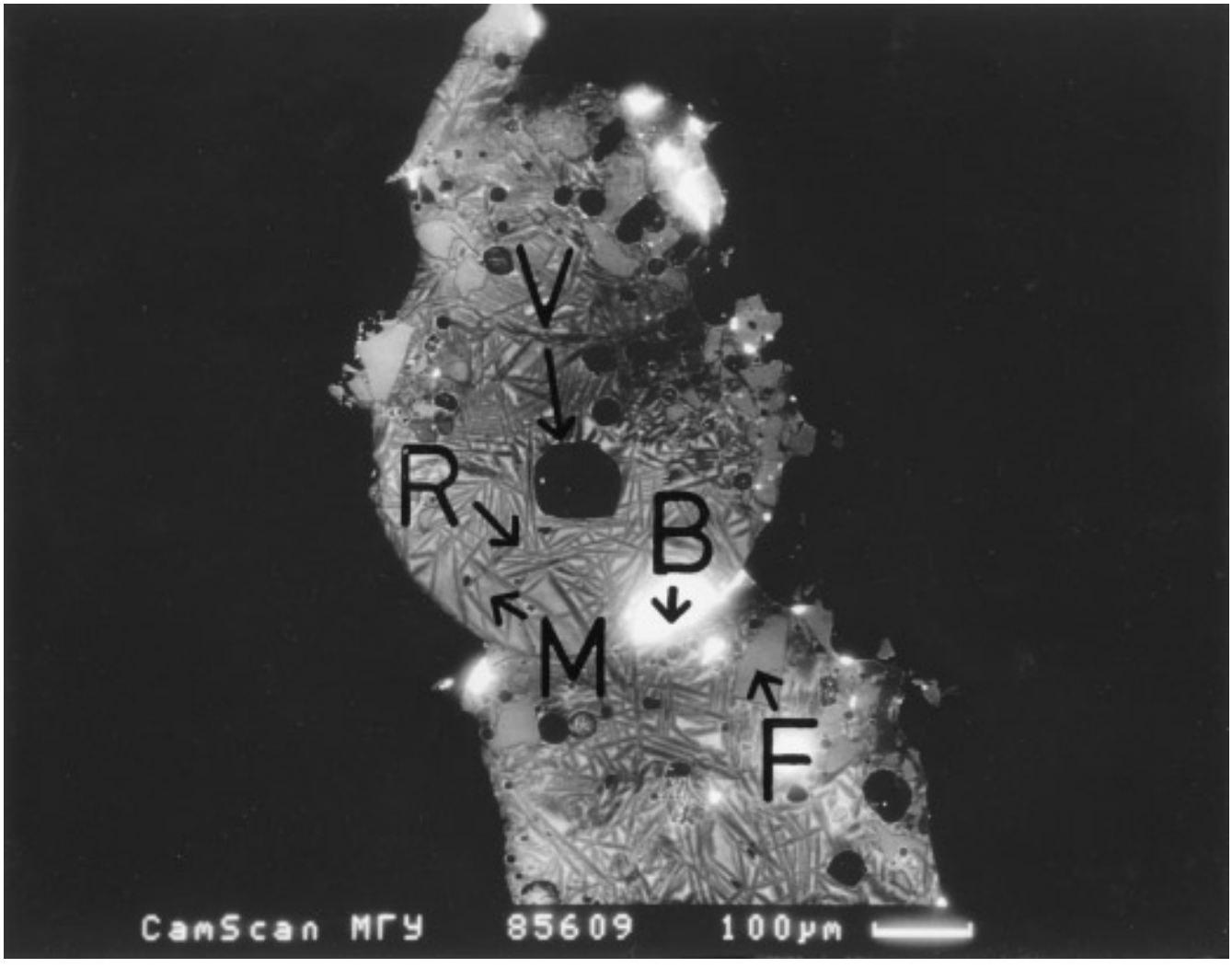

FIG. 1. BSE image of Elenovka altered material. Unfused olivine and pyroxene fragments (F) are embedded in the partly crystallized melt, which is composed of acicular skeletal Mg-rich olivine crystals (R) cemented by glassy mesostasis enriched in FeO and finely dispersed opaques (M). White areas (B) are metal/troilite beads (V) vesicles.

ples show both types of morphology (Fig. 1). All altered aggregates exhibit vesicular texture. Altered aggregates show variable amounts of unaltered powder grains stuck to their surfaces.

Altered droplets and aggregates of droplets were first examined under a binocular microscope with small magnification. Pure cpx altered droplets consist of transparent grayish-green homogeneous glass with darker areas of incipient crystallization. Pure olivine altered aggregates are characterized by uneven distribution of coloration and transparency. They exhibit areas ranging from transparent greenish-gray to ''dusty'' dark gray, almost black. Dark dusty areas show the presence of very fine-grained opaques dispersed in a translucent matrix. Ol/cpx and Elenovka altered samples are dark gray, and their thin areas (tens of micrometers) are translucent. The altered ol/cpx mixture is more light-colored and translucent than the Elenovka sample. Allende altered droplets are black and opaque and their surfaces are enriched in circular drop-like metal/sulfide inclusions.

Altered materials were studied using backscattered electron (BSE) imaging and microprobe analyses. The average microprobe analyses of various constituents of altered samples are presented in Table I. Their modal analyses calculated using BSE images are shown in Table II.

Clinopyroxene. Complete fusion appears to be attained, although altered droplets contain about 3% (by area) of unaltered grains stuck to their surfaces. The glass is largely homogeneous in appearance and composition, but contains areas of incipient crystallization of zoned cpx which is more rich in MgO than unfused cpx and glass derived from cpx (Table I). This Mg-rich cpx has thin

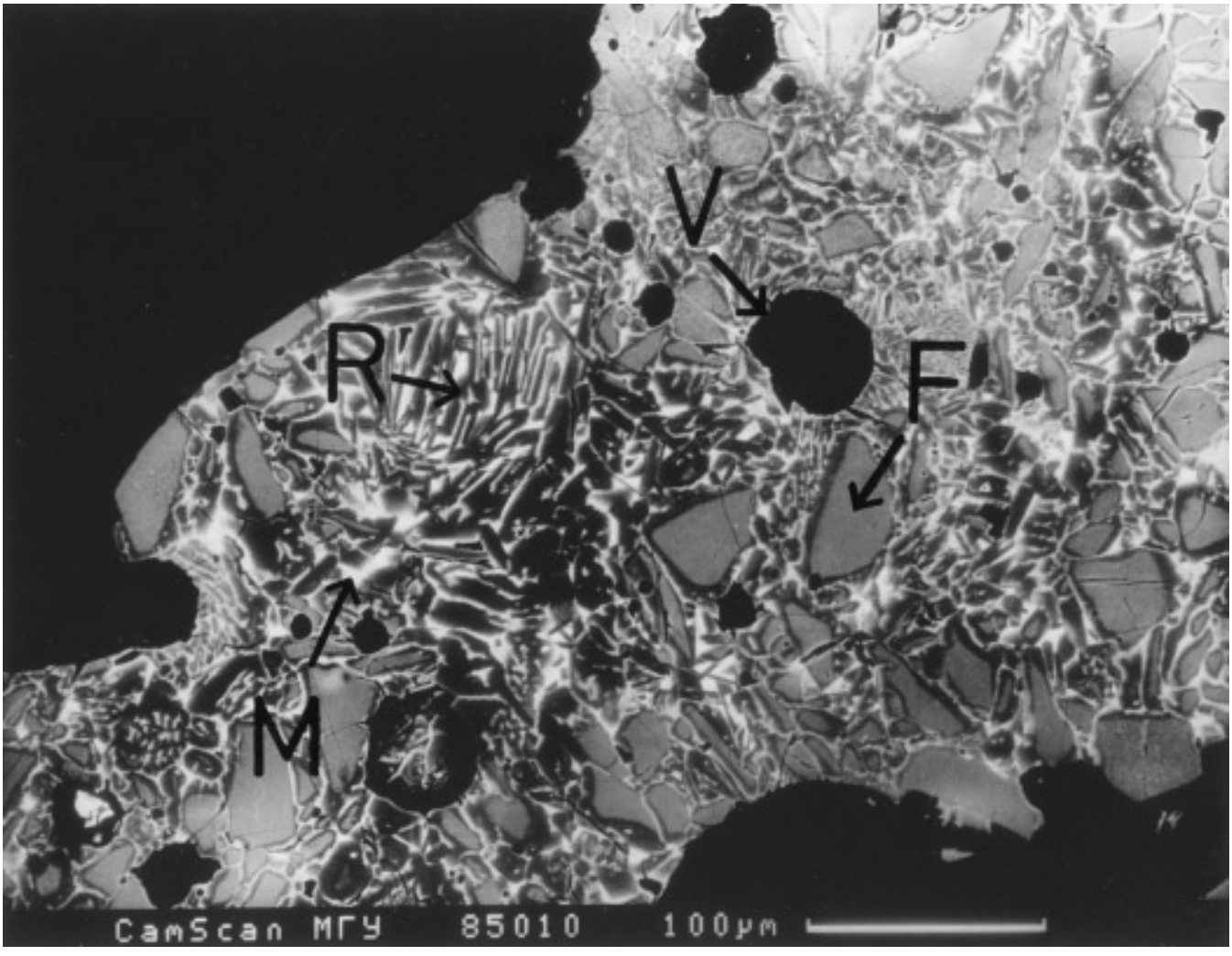

FIG. 2. BSE image of pure olivine altered material. Olivine clasts (F) are embedded in quench crystallized melt, composed of Mg-rich olivine crystals (R) cemented by Fe-rich mesostasis (M), containing numerous finely dispersed opaques. (V) vesicles.

(~1 μm) Fe-rich outer zones. The glass is slightly enriched in Al_2O_3, MgO, and FeO, and depleted in CaO and SiO_2 relative to unaltered clinopyroxene.

Olivine. Laser heating was too quick to attain complete fusion of pure olivine powder. Altered aggregates contain 36% of unfused angular clasts (usually 5–15 μm in length), whose composition is identical to that of unaltered ol. These unfused fragments (F on Fig. 2) are embedded in the melt which contains quench crystals as expected. The bulk chemistry of fused areas shows slight enrichments in CaO, Al_2O_3, and SiO_2 relative to starting material (Table I). The crystallization of the melt resulted in the formation of unequilibrated Mg-rich (Fa = 4.5 mole%) olivine crystals with very thin (0.5–1 μm) Fe-rich outer zones. The lengths of crystals range from 3 to 100 μm. Unfused clasts are rimmed by quench crystallized Mg-rich olivine. The mesostasis (M on Fig. 2) between repeatedly crystallized Mg-rich ol crystals (R on Fig. 2) is very rich in Fe and enriched in SiO_2, Al_2O_3, and CaO relative to unfused olivine and bulk melt (Table I). The mesostasis has pyroxene composition with admixture of Fe-rich phases (iron oxides or reduced iron?). The irregular inclusions (up to 2 μm) look bright (Fe-rich) on BSE images. Use of an optical microscope with high magnification ($\times$100) allows viewing of the irregular opaque inclusions which are composed of two phases with different brightness. A brighter guest phase (0.5 μm) is finely dispersed in the darker irregular host inclusions, but both Fe-phases are brighter than surrounding silicate phases. In addition, small (submicrometer) very bright single spherical opaque droplets (reduced iron?) were found on the surfaces of polished sections of altered olivine, but such droplets are much more scarce than the opaques in the mesostasis (for example, only 2 such particles were found on a surface of 0.3 mm^2).

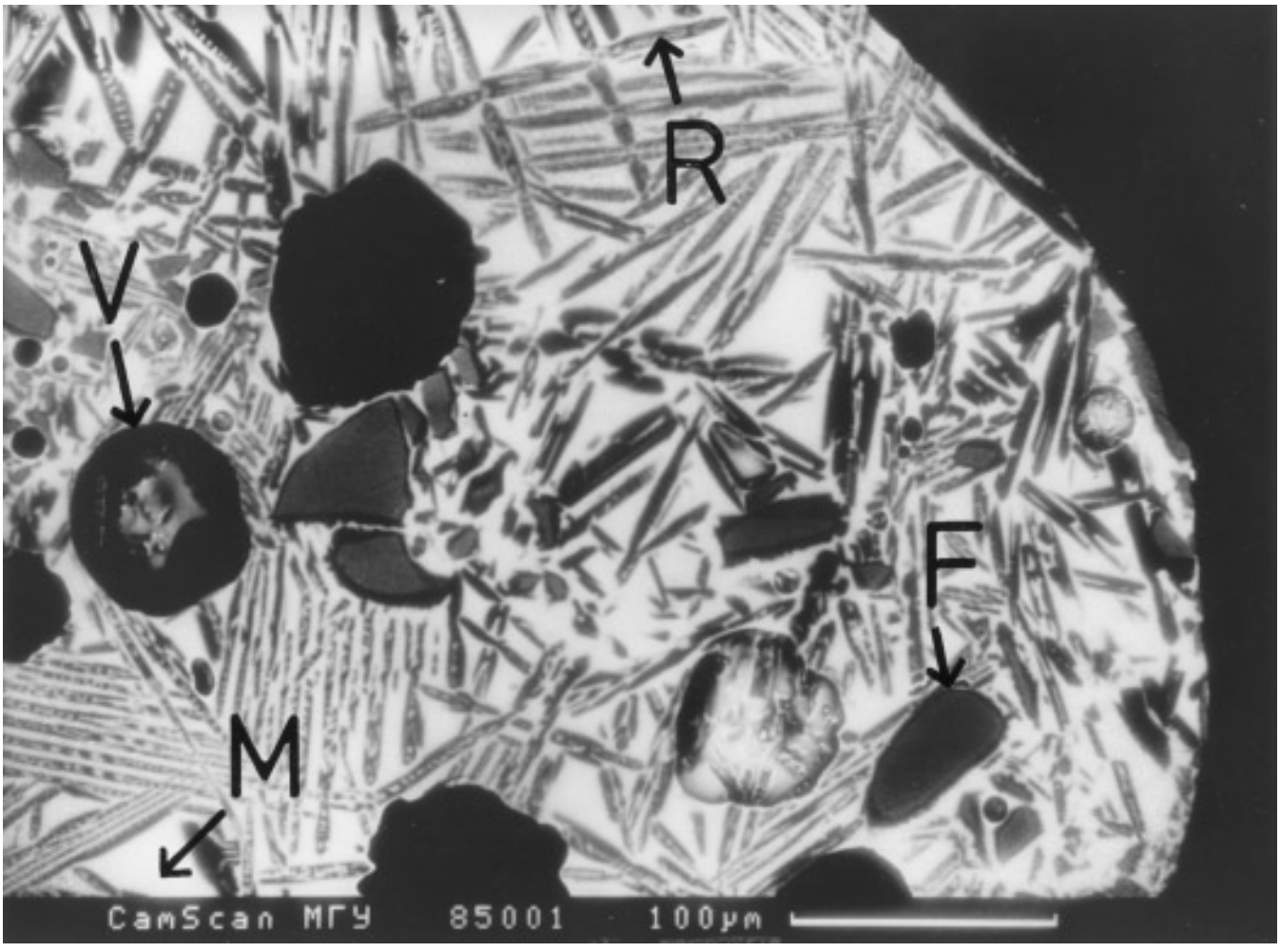

FIG. 3. BSE image of altered ol/cpx mixture (1:1). Unfused olivine fragments (F) are embedded in the partly crystallized melt, which is composed of acicular skeletal Mg-rich olivine crystals (R) cemented by glassy mesostasis enriched in FeO (M). (V) vesicles.

Unfortunately, the sizes of all opaque Fe-phases are insufficient for microprobe identification of these Fe-rich opaque phases, and we could not estimate whether our experimental conditions were reducing or not.

Examination of altered olivine aggregates in transmitted light shows that opaque phases are unevenly distributed and appear as black dust finely dispersed in the mesostasis (M on Fig. 2) between transparent unfused olivine clasts and quench crystals of olivine.

Olivine/clinopyroxene mixture (1:1). The altered sample is composed of a small amount of unfused angular olivine clasts (usually 10–15 μm; F on Fig. 3) cemented by melt. Note that cpx grains are absent among clasts. The ''melt'' is partly crystallized and shows intersertal texture with areas of barred texture (Fig. 3). Skeletal acicular ($\sim 5 \times 100$ μm) Mg-rich crystals (Fa = 4.5 mole%; R on Fig. 3) are embedded in the glassy mesostasis (M on Fig. 3). No clinopyroxenes were found among the quench crystallized phases of the melt. Interstitial glass looks homogeneous on BSE images, and is close to pure cpx in composition, but is enriched in FeO due to accumulation of FeO in the residual melt during crystallization of Fe-poor olivines upon cooling. This relatively high FeO content in the glass appears to be responsible for the darkening of the altered sample (see below). Thus, cpx constituents of the mixture were completely fused and did not crystallize upon cooling, while olivines were fused incompletely and quickly crystallized upon cooling. This last observation is very important in understanding the spectral properties of the altered ol/cpx mixture.

Elenovka. The texture of altered samples is similar to that of the ol/cpx mixture (Fig. 1). However, both olivines and pyroxenes are present among unfused fragments (F on Fig. 1). The sizes of clasts are usually 15–20 μm. Their average compositions (Table I) are identical to those of unaltered Elenovka olivines and orthopyroxenes. Unlike

the ol/cpx mixture, the altered Elenovka sample contains metal/troilite beads (up to 200 μm in diameter), indicative of the immiscibility of silicate and metal/sulfide melts. (The beads (B on Fig. 1) tend to occur close to the boundaries of glassy droplets. The melt shows intersertal and barred textures similar to those of the ol/cpx mixture. Skeletal acicular olivine crystals ($\sim 5 \times 100$ μm) are rich in Mg(Fa = 11 mole%) with very thin (0.5–1 μm) Fe-rich outer zones. These crystals (R on Fig. 1) are cemented by an Fe-rich (25% FeO) glassy mesostasis (M on Fig. 1) which looks more heterogeneous on BSE images than does the ol/cpx mixture. Besides the high FeO content, the mesostasis is enriched in Al_2O_3, TiO_2, SiO_2, and CaO (Table I). The absence of pyroxenes among repeatedly crystallized grains, and the chemical composition of the mesostasis both indicate that pyroxene portions of Elenovka silicate melt tend to accumulate in the Fe-rich residual melt, while the olivine fraction crystallized upon cooling. The cooling rate was high enough not to allow pyroxenes to crystallize. Very small (0.1–0.3 μm) Fe-rich opaque inclusions are finely dispersed in the glassy mesostasis. Some of them appear to be composed of troilite, since the bulk chemistry of the mesostasis shows increased sulfur content (Table I). Sometimes the size of opaques in the glass approaches 1 μm, but such a size is still insufficient for microprobe analysis.

Allende. The texture of altered Allende droplets is similar to that of altered Elenovka. However, pyroxene unfused clasts were not found. Olivine unfused clasts (Fa = 2–21 mole%; dominant lengths 20–40 μm) are embedded in the crystallized melt with intersertal, sometimes barred, texture. Skeletal acicular olivine crystals (Fa = 18 mole%) have thin (0.5 μm) outer zones more rich in FeO and crystal sizes are smaller (usually 10–30 μm) than those of Elenovka and the ol/cpx mixture. Besides intersertal textures, some areas exhibit microporphiritic textures. Tabular zoned ol phenocrysts (~ 5 μm) are cemented by a glassy mesostasis. These textures tend to occur in the central areas of drops. The textures of these areas indicate that the crystallization of their parent melt was slower than that of the areas with intersertal texture. Irrespective of type of texture, zoned olivine crystals are embedded in an Fe-rich (36–42% FeO) glassy mesostasis enriched in Al_2O_3, CaO, and depleted in SiO_2 relative to bulk melt composition (Table I). Similar to the Elenovka mesostasis, Allende groundmass often shows some chemical heterogeneity on BSE images and contains numerous finely dispersed Fe-rich inclusions (tenths of micrometers in size). Sometimes they approach 1 μm, and some of them are brighter than others on BSE images (probably, Fe, Ni-metal and sulfides). The increased sulfur content of mesostasis shows that sulfides are probably present.

Allende altered samples also contain metal/sulfide beads similar to those found in altered Elenovka. They also tend to occur near the boundaries of the glassy drops, but their metal shows enrichment in Ni ($\sim$30% Ni) relative to Elenovka (6–8% Ni).

Thus, except for the pure cpx sample, only partial melting has been attained as a result of laser treatment. With the exception of pure cpx, all altered materials are characterized by some common features. They contain variable amounts of unfused angular clasts embedded in the melt of intersertal texture with areas of barred texture. This melt contains at least 55% quench crystallized olivine. These acicular unequilibrated Mg-rich olivine crystals have very thin (0.5–1 μm) Fe-rich outer zones. Unfused clasts are surrounded by Mg-rich olivine rims. The Mg-rich olivines are cemented by an Fe-rich glassy mesostasis. The darkening of fused and quench crystallized samples relative to the starting materials is not difficult to explain. The cooling rate of the melt was not high enough to prevent crystallization of high-temperature Mg-rich olivines. The crystallization of Mg-rich olivines resulted in the enrichment of residual melt in FeO. However, the cooling rate was high enough to prevent the crystallization of these Fe-rich silicate melts, resulting in the formation of largely amorphous glassy mesostasis between Mg-rich olivine crystals. Fe-rich glasses are known to effectively absorb light (e.g., Adams and McCord 1970, Nash and Conel 1973, Bell *et al.* 1976). Moreover, opaque minerals are finely dispersed in the glassy groundmass of the altered Elenovka, Allende, and olivine samples. We could not identify these opaque phases in the mesostasis because of their extremely small grain sizes. The presence of even small amounts of such highly absorbing materials in optically important areas such as grain boundaries causes considerable darkening of altered samples relative to the starting materials. On the other hand, the successfully vitrified pure cpx sample did not darken.

The effects of temperature, oxygen fugacity fusion time, and techniques on glass formation are discussed elsewhere (e.g. Nash and Conel 1973, Bell *et al.* 1976, Cloutis and Gaffey 1993). Nash and Conel (1973) showed that quick-melt (on the order of seconds) glass displays more resolvable absorption bands and higher overall reflectance than slow-melt (on the order of minutes) glass. We suggest that this is the result of incomplete fusion of quick-melt materials.

4. REFLECTANCE SPECTRA OF UNALTERED AND ALTERED MATERIALS

Shown in Figs. 4–6 are bidirectional reflectance spectra of Elenovka, Allende, terrestrial olivine (ol), clinopyroxene (cpx), and an ol/cpx mixture 1 : 1 before and after laser treatment. The values of spectral parameters measured in this study are tabulated in Table III.

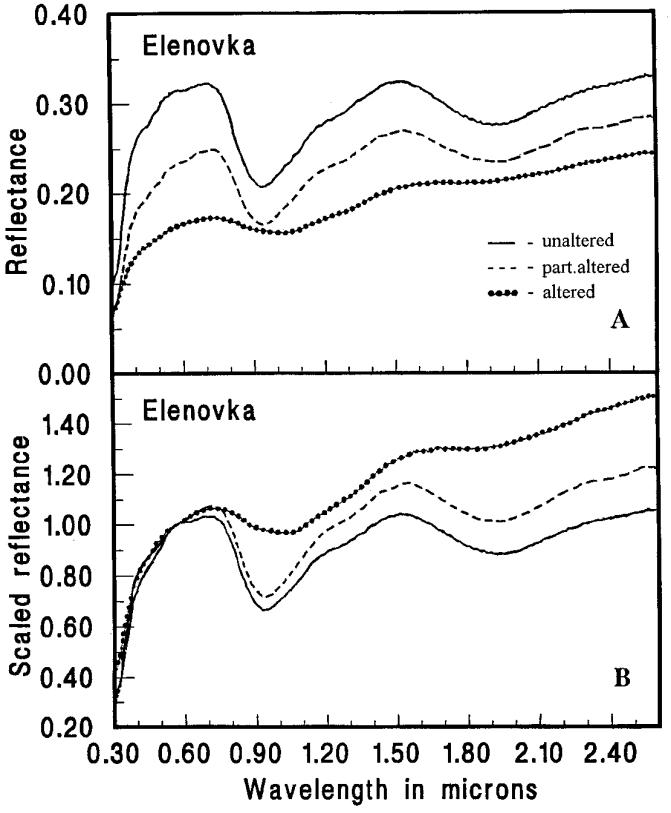

FIG. 4. Absolute VNIR reflectance spectra (A) and normalized VNIR reflectance spectra (B) of powdered Elenovka samples. The spectra in (B) have been scaled to 1.0 at 0.56 μm. Line types are consistent between (A) and (B).

The most obvious spectral changes are a drop in overall reflectance (darkening) and a reduction in spectral contrast with increasing alteration degree (Table III and Figs. 4–6). Such optical effects have been observed earlier for shocked OCs (e.g., Britt and Pieters 1990), gas-rich OCs (e.g., Britt and Pieters 1991), and fused OCs (Clark *et al.* 1992). Other interesting effects are listed below.

The continuum slope of meteorite samples reddens noticeably with increasing alteration degree. For example, the 2.5/0.56 μm reflectance ratio rises from 1.04 for the unaltered Elenovka sample to 1.49 for altered Elenovka. The 2.5/0.56 μm ratio range for Allende samples is 1.16–1.49. Similarly, the 2.5/1.8 μm reflectance ratio for the olivine series increases from 1.007 (unaltered) up to 1.086 (altered).

Alteration caused by laser shots results in the shifts in the wavelength positions of band I and band II centers (Table III). The spectra of the ordinary chondrite Elenovka are dominated by two major absorption features situated near 0.94 μm (band I) and 1.93 μm (band II).

Band I moves from 0.94 μm (unaltered) up to 1.05 (altered) for Elenovka. The content of high calcium pyroxenes in Elenovka does not exceed 5% (McSween *et al.* 1991) and should not affect the positions of band I and II (Cloutis and Gaffey 1991). So, the meteorite Elenovka may be roughly described as a two-component mixture of olivine Fa_{25-26} (mole%) and orthopyroxene Fs_{19-23} (mole%) (Baryshnikova and Lavrukhina 1979). For such mixtures, the band I wavelength position is a function of relative abundance and composition of olivine and orthopyroxene phases. Band I is known to move toward longer wavelength with increasing olivine abundance as well as increasing ferrous iron content of the ol/opx mixtures (Cloutis *et al.* 1986).

A lesser shift to longer wavelength with increasing alteration degree is observed for band II (Table III), but this can be attributed to distortion of band shape from sloping spectral background, and not necessarily from changes in mineralogy. Band II position is sensitive to Fs content of orthopyroxene (Adams 1974). According to the calibration of Adams (1974) later corrected by Gaffey (1984), the Fs content of unaltered orthopyroxene of the Elenovka meteorite is 36 wt% (Table III). This value agrees with the chemically measured Fs content of Elenovka orthopyroxene—37 wt% (Baryshnikova *et al.* 1985). This agreement

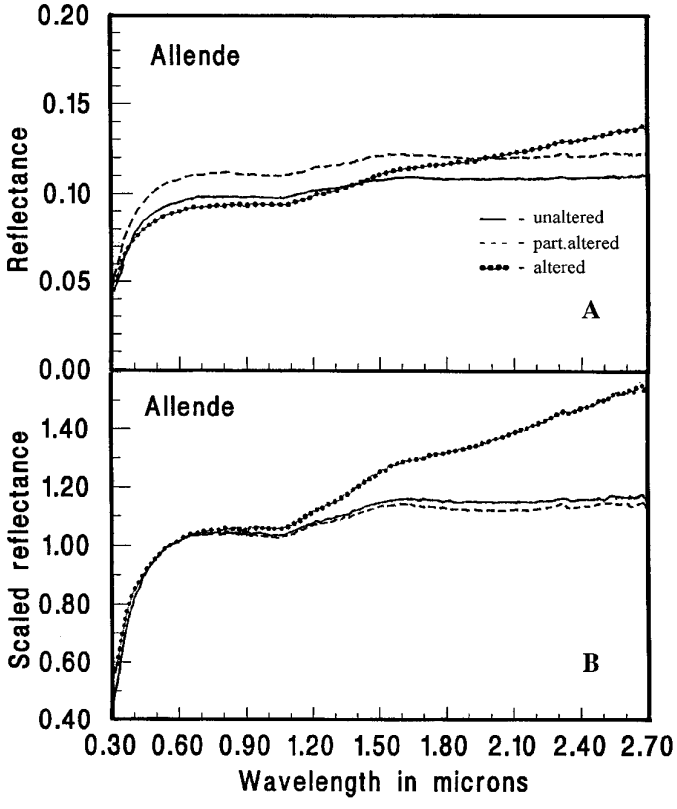

FIG. 5. Absolute VNIR reflectance spectra (A) and normalized VNIR reflectance spectra (B) of powdered Allende samples. The spectra in (B) have been scaled to 1.0 at 0.56 μm. Line types are consistent between (A) and (B).

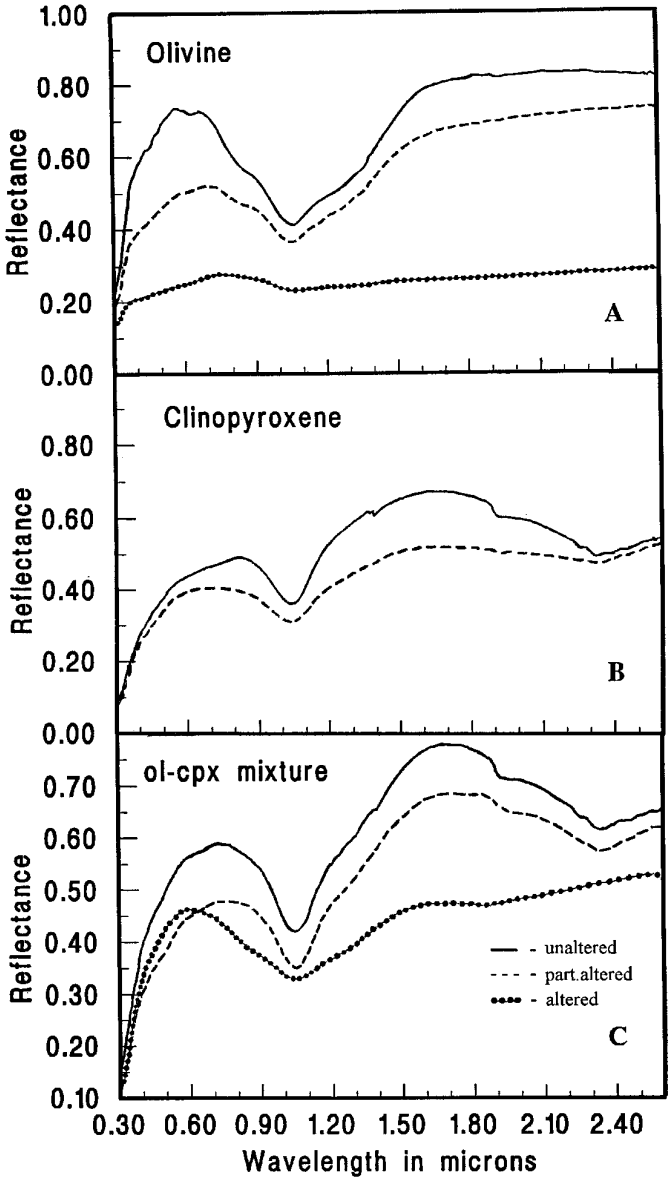

FIG. 6. Absolute VNIR reflectance spectra of powdered olivine (A), pyroxene (B) samples, and ol/cpx mixture (C). Line types are consistent between (A), (B), and (C).

indicates that the presence of small amounts of high calcium pyroxenes in Elenovka does not affect the band II position.

Similarly, the reflectance spectra of pure olivine exhibit a slight migration of band I center from 1.055 to 1.072 μm as a result of alteration (Table III). The 1 μm absorption band of olivine is known to move to longer wavelength with increasing iron content (Burns 1970a).

The less prominent 1 μm olivine absorption feature in the spectrum of Allende also appears to shift to slightly longer wavelength after laser treatment (from 1.06 to 1.08 μm).

An additional broad shallow absorption feature centered near 1.9 μm appears in the spectrum of the altered Allende sample (Fig. 5). A similar broad absorption is present in the spectra of altered pure olivine and altered ol/cpx mixture. In the spectrum of the altered ol/cpx sample this feature seems to overlap the OH^- absorption band situated near 1.9 μm. The appearance of an additional broad absorption near 1.9 μm is probably associated with the formation of Fe-bearing glass as the result of laser treatment (Bell *et al.* 1976). A similar broad shallow band was also observed in the spectrum of fused carbonaceous chondrite Murchison (CM2) published by Clark *et al.* (1993).

The modified Gaussian model (MGM) has been employed to deconvolve VNIR reflectance spectra of the pure olivine series, following the procedure outlined by Sunshine *et al.* (1990). The spectra of unaltered and partly altered samples were fit successfully using this method (Fig. 7). The results indicate that the increase in the continuum slope is sufficient to fit the special curve of partly altered olivine. However, an additional component, probably Fe^{+2}-bearing glass (Bell *et al.* 1976, Cloutis and Gaffey 1993), is indicated by deconvolution of the spectrum of the more altered sample, as represented by two broad shallow bands centered near ~1 and 1.9 μm (see Fig. 6c).

Not only absorption bands change in wavelength position due to laser impulse alteration; other spectral parameters such as reflectance peaks also change. An increase in the wavelength position of the local reflectance maximum between band I and band II (interband peak) is observed for Elenovka samples after laser treatment (Table III). Similarly, the local reflectance maximum in the 0.5–0.8 μm spectral region (0.7 μm peak) moves to longer wavelengths with increasing alteration in the Elenovka and pure olivine samples (Table III).

The 2 μm/1 μm (BII/BI) area ratio for the Elenovka series decreases as a result of alteration. The BII/BI area ratio is primarily a function of relative abundance of olivine and orthopyroxene phases (Cloutis *et al.* 1986). The BII/BI area ratio makes it possible to estimate the ol/opx ratio in two-component olivine–orthopyroxene mixtures. The spectrally derived ol/px ratio increases from 2.8 for the unaltered Elenovka sample to 5.4 for the altered one. A similar trend is observed for the olivine–clinopyroxene mixture. The clinopyroxene absorption feature (band II) near 2.3 μm disappears in the spectrum of the altered ol/cpx sample.

The majority of measured mid-infrared spectra are not discussed in this paper, but some of them are important for the understanding of our main results.

All mid-IR spectra of meteorites and minerals discussed here have spectral features associated with volume scattering in the 4.5 to 7 μm region. These features appear to be overtones of the fundamental molecular vibration bands, or the combination tones of the fundamentals with lattice

TABLE III
Various Spectral Parameters Used in This Study

Sample	Band I center	Band II center	Band I depth[a]	$R_{0.56}$	Tangent intercept	Peak at 0.7 μm	BII/BI ratio	$\frac{\text{opx}}{\text{opx + ol}}$ (wt%)[b]	ol/opx ratio[b]	Fs[b]
					Elenovka (*L*5) series					
unaltered	0.940	1.934	0.363	0.31	1.48	0.71	0.501	26.1	2.8	36
part. alt.	0.942	1.936	0.349	0.23	1.37	0.72	0.491	25.7	2.9	36
altered	1.051	1.963	0.160	0.16	1.22	0.75	0.250	15.6	5.4	44
					Allende (CV3) series					
unaltered	1.061		0.049	0.094						
part. alt.	1.056		0.047	0.107						
altered	1.084		0.075	0.089						
					Olivine series					
unaltered	1.055		0.452	0.73	1.54	0.57				
part. alt.	1.059		0.368	0.49	1.38	0.70				
altered	1.072		0.174	0.24	2.27	0.75				
					Clinopyroxene series					
unaltered	1.041	2.325	0.341	0.55	1.16	0.49				
part. alter	1.039	2.325	0.316	0.53	1.20	0.41				
					Olivine–Clinopyroxene (1:1) series					
unaltered	1.047	2.324	0.363	0.55	1.27	0.73				
part. alt.	1.048	2.325	0.361	0.44	1.22	0.76				
altered	1.046	1.886	0.296	0.46	1.52	0.60				
68 Leto[c]	1.045 ±.015	1.940 ±.040	0.140 ±.010	0.20 ±.01						

[a] Clark and Roush (1984).
[b] All parameters are spectrally derived.
[c] From Gaffey *et al.* (1993).

modes at longer wavelength (Salisbury 1993). Minerals such as olivine and pyroxene display quite strong and distinctive features in this spectral range. Pure olivine samples have a series of absorptions between 4.95 and 6.25 μm with the most prominent located at 5.63 and 6.01 μm (Fig. 8(5)). The shapes of pure clinopyroxene absorption features (Fig. 8(4)) are typical of pyroxenes and can be easily distinguished from those of olivines. The most intense absorptions occur at 5.08 and 6.11 μm.

The spectral behavior of the ol/cpx mixture is very interesting in the spectral region 3–25 μm. The spectra of unaltered and partly altered samples display a series of overlapping olivine and clinopyroxene absorption bands, with pyroxene absorptions being more prominent as two troughs at ~5 and ~6 μm (Figs. 8(1) and 8(2)). However, clinopyroxene absorption bands practically disappear in the spectrum of the most altered sample, and the shape of the resulting features becomes very similar to that of pure olivine (Fig. 8(3)). Thus, an apparent disappearance of clinopyroxene is observed as a result of laser alteration.

5. DISCUSSION AND CONCLUSIONS

The data indicate that the majority of spectral parameters which appear to be diagnostic of composition and abundance variations are affected by quick melting and quench crystallization.

On one hand, the variations of the spectral parameters mentioned above serve as indicators of the changes in mafic mineral compositions and relative mineral abundances. On the other hand, the addition of glass to mafic mineral assemblages can affect all of the important spectral parameters. This is evident from the data of Cloutis and Gaffey (1993), who found that the addition of glass to a mafic silicate-bearing mixture results in a reduction in overall reflectance, band depths, and band area ratios, a general decrease in band II wavelength position, and an increase in interband peak position. An increase in overall continuum slope was also observed as the result of increasing glass content. Cloutis and Gaffey's (1993) mixture GF9 containing olivine, orthopyroxene, and smaller amounts of

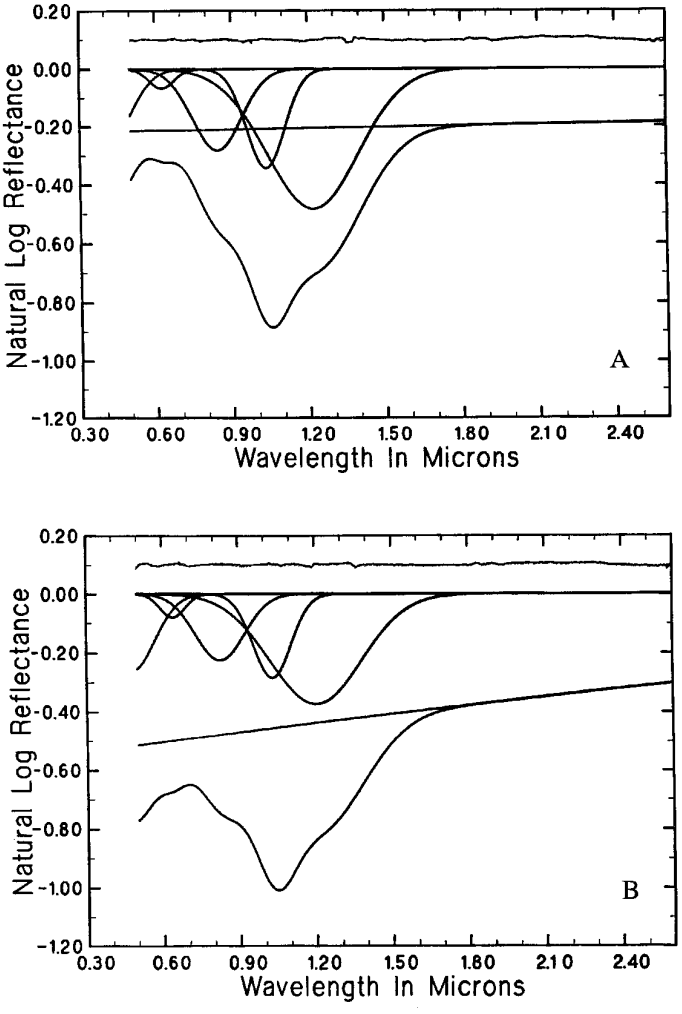

FIG. 7. The Gaussian model of the olivine reflectance spectra (particle size <75 μm). (A) Unaltered sample; (B) Partly altered sample. The model components are (from bottom to top): the modeled spectrum superimposed on the reflectance spectrum, the continuum, the individual Gaussian distributions that comprise the model, and the residual error between the model and the actual spectra (offset 10% for clarity).

plagioclase and ilmenite could be considered as a spectral analog of the Elenovka meteorite. However, the addition of glass to that mixture decreases the wavelength positions of band II and the interband peak, while the laser treatment of Elenovka results in the opposite effects (Table III).

We think that knowledge of the cooling rate is critical to understanding the unusual spectral properties of altered samples which contain both olivines and pyroxenes. The petrographic and chemical analyses of altered materials in Section 3 demonstrate that quick melting and cooling of ol,px-bearing melts result in the crystallization of *olivines*, while the pyroxene fraction of the melt tends to accumulate in the glassy mesostasis. This mesostasis appears to be largely amorphous, resulting in the disappearance of pyroxene absorption features in the spectra of ol,px-bearing altered materials. This results in the displacement of band I to longer wavelength, the increase in BII/BI ratio, and, consequently, in the increase in spectrally derived ratios of olivine to pyroxene.

Interestingly, the melted and quench crystallized ordinary chondrite samples prepared by Clark *et al.* (1992) do not show such effects. We suggest that their samples cooled more slowly because of the larger sizes of their fused specimens. We have also compared our results with the petrographic work of Zinovieva *et al.* (1994), who studied a more slowly fused and cooled sample of Tsarev (*L5*) OC. Their results show that such slower melting and cooling caused crystallization of both olivines and pyroxenes, while in our Elenovka and ol/cpx samples only olivines were quench crystallized. Moreover, our altered ol/cpx samples demonstrate that the fusion of pyroxene grains was also more effective than fusion of olivines. No pyroxene clasts were found among unfused fragments of altered ol/cpx mixture. Thus, very quick cooling (on the order of a few seconds) appears to be needed to obtain results similar to ours.

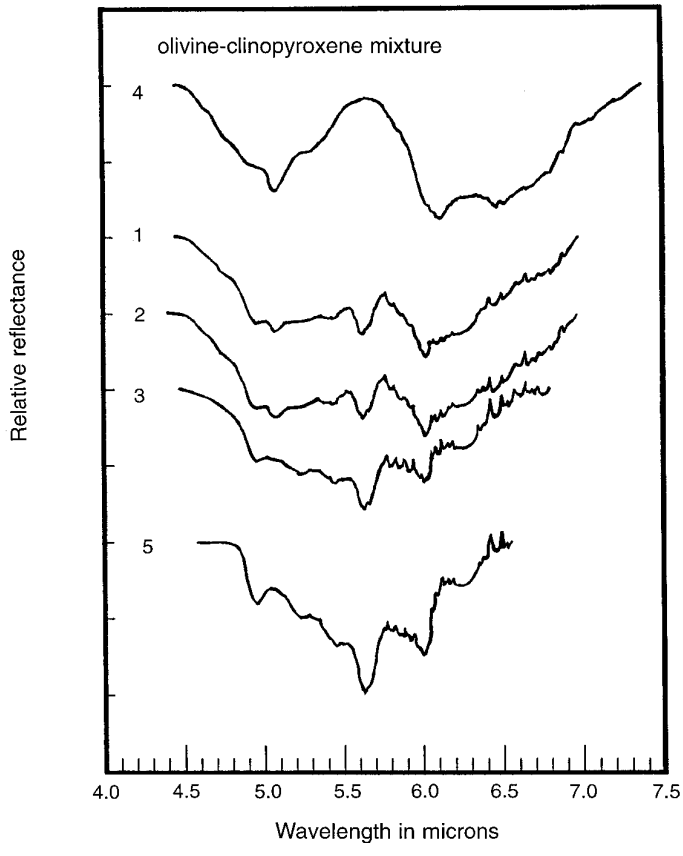

FIG. 8. Biconical reflectance spectra of the olivine–clinopyroxene mixture in the range 4.5–7.5 μm (offset 20% between (1), (2), (3); and 40% between (4) and (1), (3) an (5)). (1) Unaltered ol/cpx sample; (2) partly altered ol/cpx sample; (3) altered ol/cpx sample; (4) unaltered cpx sample; (5) altered ol sample.

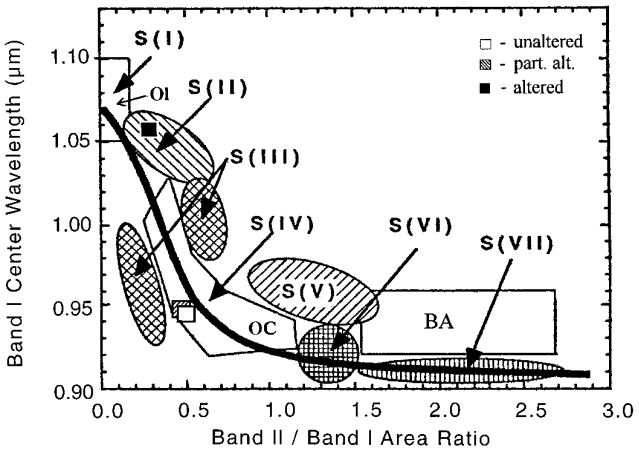

FIG. 9. Plot of the band I center versus the band II/band I area ratio for Elenovka series relative to the S-asteroid subtypes and three types of meteorite assemblages (from Gaffey *et al.* 1993). The OL rectangular region encompasses essentially monomineralic olivine assemblages. The OC polygonal region represents the mafic silicate components of ordinary chondrites. The BA rectangular zone includes the pyroxene-dominated basaltic achondrites. The heavy solid line indicates the location of the olivine–orthopyroxene mixing line (Cloutis *et al.* 1986).

The reasons for the darkening of our altered materials were discussed in Section 3. We think that the accumulation of FeO in the interstitial residual melt due to crystallization of Mg-rich olivine crystals and finely dispersed opaques are responsible for this process.

The red slopes of our altered samples may be due to the presence of Fe-bearing glasses (Adams and McCord 1970, Nash and Conel 1973, Bell *et al.* 1976). We suggest that the less steep spectral slopes of fused OC samples prepared by Clark *et al.* (1992) can be explained by the fact that experimental conditions were different from ours (fusion time, cooling rate, etc.). It is possible that their altered samples contain a lesser amount of amorphous material. It is possible that reduced iron is finely dispersed in the glassy mesostasis of our altered samples and results in their spectral reddening, but we cannot prove it. Troilite is also a spectrally red component and could cause spectral reddening of altered meteorite samples if it were finely dispersed in their interstitial glassy component.

The displacements of absorption features which were sometimes observed in the spectra of altered materials can be attributed to the overlapping absorption bands of various Fe-bearing silicates and glass (e.g., Farr *et al.* 1980).

Implications for S-type Asteroids

One of the most important results of this work is the ''disappearance'' of pyroxene spectral features in the spectra of altered ol,px-bearing assemblages. This effect is revealed both in the near-infrared and in the mid-infrared spectral regions. The significance of this effect for the interpretation of S-asteroid spectra is illustrated in Fig. 9. Shown in Fig. 9 are the band I centers plotted relative to BII/BI area ratios for seven spectral subtypes of S-asteroids compared to the same parameters of ordinary chondrites, achondrites (adapted from Gaffey *et al.* 1993a), and the Elenovka series. Gaffey *et al.* (1993a) have demonstrated that only asteroids assigned to the subtype S(IV) are characterized by silicate spectral properties comparable to those of ordinary chondrites. The points for Elenovka OC on the plot shows a shift from the ''chondritic'' field (unaltered sample) to the field of olivine-rich S(II)-asteroids (altered sample). Laser impulse alteration raises the spectrally derived ol/opx ratio up to 5.4. This value is far outside the OC range (~0.6–3.5 according to McSween *et al.* 1991), but falls within the ol/opx range for S-type asteroids (usually 1.5–6.0 according to Gaffey *et al.* 1990).

The normalized spectra of the Elenovka series are shown in Fig. 10 compared to the spectral reflectance curve of the asteroid 68 Leto assigned to the subtype S(II) by Gaffey *et al.* (1993a). The spectrum of 68 Leto differs significantly from that of the unaltered Elenovka sample. However, the spectral slope as well as the band I and band II positions, BII/BI ratio, and band I depth of 68 Leto (Table I) are comparable to those of the altered Elenovka sample (curve 3 on Fig. 10).

The relation between albedo, spectral slope, and band I depth are illustrated in Fig. 11 for 39 S-type asteroids (from Fanale *et al.* 1992) and for the Elenovka series. The points for unaltered Elenovka are outside the field of S-type asteroids. Fanale *et al.* (1992) showed that the same situation is typical for other OCs. However, the altered Elenovka sample falls within the field of S-asteroids with respect to all three parameters.

The results suggest that quick melting and quench crystallization can enhance the spectral similarity between S-

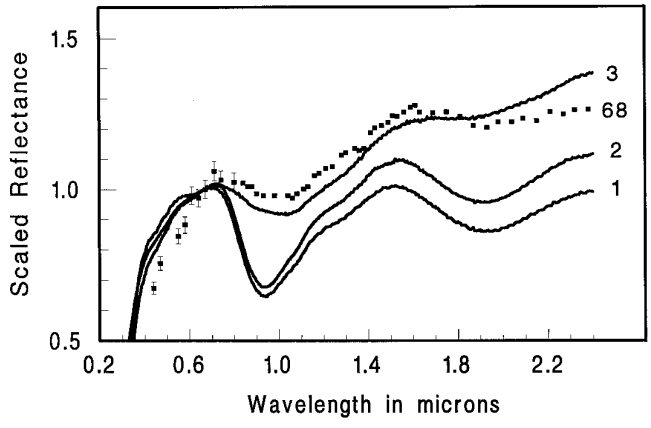

FIG. 10. Normalized reflectance spectra of S-asteroid 68 Leto (from Bell *et al.* 1988, Zellner *et al.* 1985) and the series of Elenovka samples (particle size <75 μm). The spectra have been scaled to 1.0 at 0.65 μm. (1) Unaltered sample; (2) partly altered sample; (3) altered sample; (68) Leto.

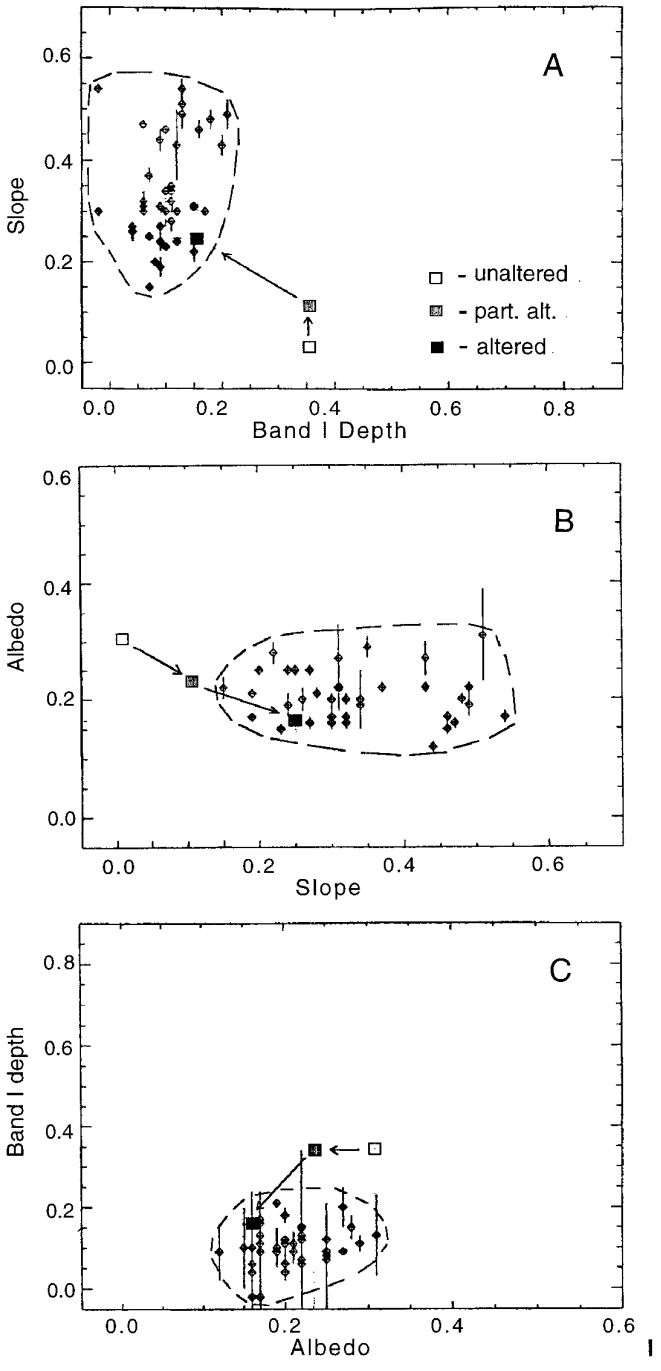

FIG. 11. The plots of the spectral parameters (slope, band I depth, albedo) for 39 asteroids (from Fanale *et al.* 1992) and the Elenovka series. The fields of S-asteroids on the plots are outlined by the dashed lines.

type asteroids and ordinary chondrites in terms of spectral slope, albedo, band depths, and spectrally derived ol/opx ratio.

However, there are other spectral properties of some S-asteroids, that are known to contradict the space weathering hypothesis of the OC origin. Two large S-type objects, 8 Flora and 15 Eunomia, have shown unusual spectral variations along their surfaces. Gaffey (1984) and Gaffey and Ostro (1987) have demonstrated that these two asteroids are characterized by a positive correlation between the band II positions and BII/BI area ratios, which is opposite to the negative correlation of the same parameters for various OC groups (McSween 1992). The data for the Elenovka series obtained in this study are also inconsistent with the rotational variations on the surfaces of 8 Flora and 15 Eunomia. Nevertheless, more extensive data on glass-bearing mixtures of mafic minerals obtained by Cloutis and Gaffey (1993) show that the addition of glass to mafic mineral assemblages is usually accompanied by simultaneous decrease in band area ratio and band II wavelength position. Thus the observed spectral variations along the surfaces of Flora and Eunomia can possibly be explained by spatial variations of impact glass abundance.

It is generally accepted that the formation of glass on asteroidal surfaces should be largely inhibited (Hörz and Schaal 1981, McKay *et al.* 1989). However, the possibility of such a process has not been disproven and should be taken into consideration.

Galileo SSI color data between 0.4 and 1.1 μm (Belton *et al.* 1994) show the probable evidence of optical alteration due to space weathering on the surface of the S-type asteroid 243 Ida. On Ida, a distinct regional inhomogeneity was noted by the Galileo Imaging Team (Helfenstein *et al.* 1994). Small but significant color variations are correlated with albedo: brighter areas have deeper 1-μm absorption and "bluer" colors than darker areas. Such a correlation is generally consistent with a slight degree of optical alteration in a regolith which is less mature on steep slopes and in fresher craters.

The data discussed in the present paper probably do not allow for all of the diversity of S-asteroids to be explained. In addition, it is difficult to account for the recently discovered relationship between the spectral slopes of S-asteroids and their diameters in terms of the space weathering hypothesis (Gaffey *et al.* 1993b).

Nevertheless, the data obtained in this study increase the number of possible candidates of OC parent bodies among the main belt population of S-type asteroids. Thus, a regolith processed OC-like material may be present on the surfaces of S-asteroids, if we assume that these surfaces contain melted and quench crystallized impact products such as those produced by these experiments.

Implications for Low-Albedo Asteroids

The low-albedo asteroids (C, B, G, F, P, D, T-types) appear to be enriched in opaque materials. Unlike S-types, their spectral reflectance curves are relatively featureless. Such optical characteristics make it difficult to establish reliable genetic links between specific meteorites and low-

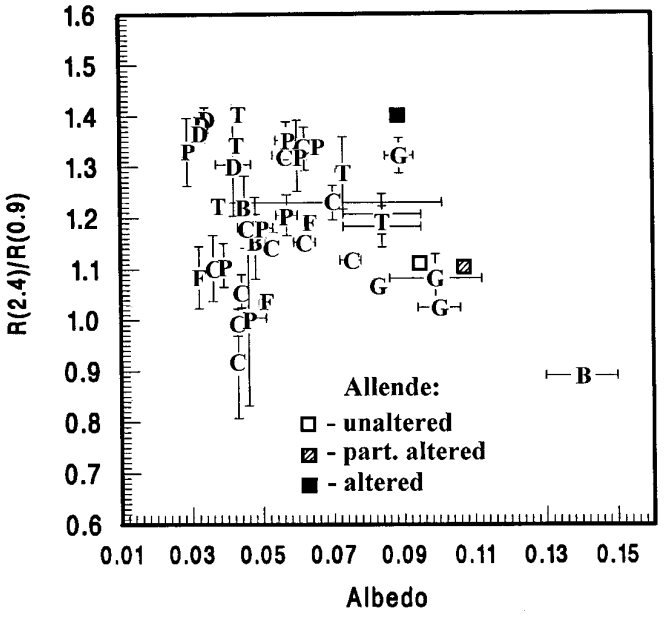

FIG. 12. Plot of the $R_{2.4}/R_{0.9}$ ratios (from Bell *et al.* 1988) versus IRAS albedos (from Tedesco 1989) for 37 low-albedo asteroids and the series of Allende samples. Error bars represent one standard deviation in the calculation of the parameters.

albedo asteroids. Moreover, the possible effects of space weathering on the surfaces of dark asteroids are not well understood.

Carbonaceous chondrites are traditional meteorite analogs of dark asteroids, though black ordinary chondrites spectrally resemble some C-class objects (Britt and Pieters 1987). The impulse laser alteration of carbonaceous chondrite Allende (CV3) results in the marked reddening of its VIS–NIR continuum (Fig. 5). Slope variations are typical of the dark asteroid population (e.g., Feierberg *et al.* 1985, Vilas and Smith 1985, Britt *et al.* 1992). Whatever the reasons of these slope variations, the possible contribution of surface altering processes should not be ignored when interpreting such spectral differences.

The relation between NIR spectral slope ($R_{2.4}/R_{0.9}$) and albedo is shown in Fig. 12 for 37 low-albedo asteroids and for the Allende series. The spectrum of the altered Allende sample is more red-sloped than the majority of C, B, F, G-type asteroids. The near-infrared spectral slope for the altered Allende sample is similar to those of some P, D, and T-type asteroids, but these objects are darker and do not have a deep UV fall-off, which is typical of all Allende samples and other carbonaceous chondrites (Tholen 1984, Hiroi *et al.* 1995). The closest approximation to the red slope of altered Allende among dark asteroids with deep UV fall-off are the G-types 130 Electra and 19 Fortuna (the latter is not shown on the plot because of the lack of albedo information). It should be noted that such optical parameters as slopes and albedos are not very conclusive, since they may depend not only on composition, but also on physical parameters, such as particle (or grain) sizes. For example, the grinding of carbonaceous chondrites increases their albedos, band depths, and spectral slopes (Johnson and Fanale 1973, Moroz and Pieters 1991). C, B, F, and G-type low-albedo asteroids are known to have systematically bluer slopes and weaker UV absorption bands than carbonaceous chondrites (Britt *et al.* 1992), Hiroi *et al.* 1993b). The data on altered Allende demonstrate that optical alteration due to impact melting and subsequent crystallization is not a likely mechanism to explain the spectral mismatch between dark asteroids and carbonaceous meteorites, since the spectrum of the altered Allende sample is too red-sloped. Hiroi *et al.* (1993b) showed that thermal metamorphism of low-albedo asteroids may account for the spectral differences between these objects and carbonaceous chondrites.

Thus, the results obtained in this study show that regolith processes such as impact melting and quench crystallization could affect optical properties of the surfaces of atmosphereless bodies more heavily than has previously been appreciated. In particular, the results indicate that the pyroxene spectral signatures may partly or completely "disappear" in the spectra of olivine, pyroxene-bearing assemblages due to impact melting and subsequent crystallization of olivine. This process might result in increased spectrally derived olivine/pyroxene ratios. The data obtained in this study demonstrate that the reflectance spectra of atmosphereless bodies should be interpreted with great caution, especially when impact glass formation and/or quench crystallization is anticipated.

ACKNOWLEDGMENTS

We are grateful to Stephen Pratt for the measurements of the reflectance spectra at the NASA RELAB bds and Nicolet 740 FTIR spectrometer facilities at Brown University. Thanks also to Dr. Jessica Sunshine for her help with MGM analysis. We are grateful to Dr. N. G. Zinovieva and Dr. A. A. Ulyanov for their help with SEM studies and microprobe analyses. The specimens of meteorites were kindly provided by the Committee on Meteorites of the Russian Academy of Sciences. We thank Dr. Beth Clark and an anonymous reviewer for their thoughtful reviews. This work was partly supported by a grant from the American Astronomical Society, and NASA Grant NAGW-28.

REFERENCES

Adams, J. B. 1974. Visible and near-infrared diffuse reflectance spectra of pyroxenes as applied to remote sensing of solid objects in the Solar system. *J. Geophys. Res.* **79,** 4829–4836.

Adams, J. B., and T. B. McCord 1970. Remote sensing of lunar surface mineralogy: implications from visible and near-infrared reflectivity of Apollo 11 samples. *Proc. Apollo 11 Lunar Sci. Conf.* **3,** 1937–1945.

Allen, C. C., R. V. Morris, H. V. Lauer, Jr., and D. S. McKay 1993. Microscopic iron metal on glass and minerals—a tool for studying regolith maturity. *Icarus* **102,** 291–300.

Baryshnikova, G. V., and A. K. Lavrukhina 1979. Investigation of the Elenovka chondrite (the petrology and mineralogy). *Meteoritika* **38,** 37–45. [Russian]

Baryshnikova, G. V., S. A. Stakheeva, K. I. Ignatenko, and A. K. Lavrukhina 1985. Pyroxenes of ordinary chondrites of H- and L-groups. *Geokhimia* **1,** 20–34. [Rusian]

Bell, J. F., and K. Keil 1988. Spectral alteration effects in chondritic gas-rich breccias: Implications for S-class and Q-class asteroids. *Proc. 18th Lunar Planet. Sci.,* 753–780.

Bell, P. M., H. K. Mao, and R. A. Weeks 1976. Optical spectra and electron paramagnetic resonance of lunar and synthetic glasses: A study of the effects of controlled atmosphere, composition and temperature. *Proc. Lunar Sci. Conf. 7th,* 2543–2559.

Bell, J. F., D. R. Davies, W. K. Hartmann, and M. J. Gaffey 1989. Asteroids: the big picture. In *Asteroids II* (R. P. Binzel, T. Gehrels, and M. S. Matthews, Eds.), pp. 921–945, Univ. of Arizona Press, Tucson.

Bell, J. F., P. D. Owensby, B. R. Hawke, and M. J. Gaffey 1988. The 52-color asteroid survey: Final results and interpretation. *Lunar Planet. Sci. XISX,* 57–58.

Belton, M. J. S., C. R. Chapman, J. Veverka, K. P. Klaasen, A. Harch, R. Greeley, R. Greenberg, J. W. Head, A. McEwen, D. Morrison, P. C. Thomas, M. E. Davis, M. H. Carr, G. Neukum, F. P. Fanale, D. R. Davis, C. Anger, P. J. Gierasch, A. P. Ingersoll, and C. B. Pilcher 1994. First images of asteroid 243 Ida. *Science* **265,** 1543–1547.

Binzel, R. P., S. Xu, J. Bus, M. F. Skrutskle, M. R. Meyer, P. Knezek, and Barker E. S. 1993. Discovery of a main belt asteroid resembling ordinary chondrite meteorites. *Science* **262,** 1541–1543.

Britt, D. T., and C. M. Pieters 1991. Darkening in gas-rich ordinary chondrite parent bodies. *Lunar Planet. Sci. XXII,* 129–130.

Britt, D. T., and C. M. Pieters 1987. The optical effects of surface processes on small bodies. *Meteoritics* **22,** 340–342.

Britt, D. T., and C. M. Pieters 1990. The spectral effects of dispersed opaques in optically altered ordinary chondrites. *Lunar Planet. Sci. XXI,* 127–128.

Britt, D. T., D. T. Tholen, J. F. Bell, and C. M. Pieters 1992. Comparison of asteroid and meteorite spectra: classification by principal component analysis. *Icarus* **99,** 153–166.

Burns, R. G. 1970a. Crystal field spectra and evidence of cation ordering in olivine minerals. *Am. Miner.* **55,** 1608–1632.

Burns, R. G. 1970b. *Mineralogical Applications to Crystal Field Theory.* Cambridge Univ. Press, New York.

Cassidy, W., and B. Hapke 1975. Effects of darkening processes on surfaces of airless bodies. *Icarus* **25,** 371–383.

Clark, B. E., F. P. Fanale, and M. S. Robinson 1993. Simulation of possible regolith optical alteration effects on carbonaceous chondrite meteorites. *Lunar Planet. Sci. XXIV,* 301–302.

Clark, B. E., F. P. Fanale, and J. W. Salisbury 1992. Meteorite–asteroid spectral comparison: The effects of comminution, melting and recrystallization. *Icarus* **97,** 288–297.

Clark, R. N., and T. L. Roush 1984. Reflectance spectroscopy: Quantitative analysis techniques for remote sensing applications. *J. Geophys. Res.* **89,** 6329–6340.

Cloutis, E., and M. Gaffey 1991. Spectral-compositional variations in the constituent minerals of mafic and ultramafic assemblages and remote sensing implications. *Earth, Moon, Planets* **53,** 11–53.

Cloutis, E. A., and M. J. Gaffey 1993. Lunar regolith analogues: Spectral reflectance properties of compositional variations. *Icarus* **102,** 203–224.

Cloutis, E. A., M. G. Gaffey, T. L. Jakowski, and K. L. Reed 1986. Calibrations of phase abundance, composition, and particle size distribution for olivine–orthopyroxene mixtures from reflectance spectra. *J. Geophys. Res.* **91,** 11641–11653.

Danielson, L. R., and R. H. Jones 1995. Experimental reduction of olivine: constraints on formation of dusty relict olivine in chondrules. *Lunar Planet. Sci. XXVI,* 309–310.

Dikov, Yu. P., O. I. Yakovlev, M. V. Gerasimov, and F. Wlotzka 1994. High-temperature vaporization of olivine and serpentine. *Lunar Planet. Sci. XXV,* 329–330.

Fanale, F. P., B. E. Clark, and J. F. Bell 1992. A spectral analysis of ordinary chondrites, S-type asteroids, and their component minerals: Genetic Implications. *J. Geophys. Res.* **97**(E12), 20863–20874.

Farr, T. G., B. A. Bates, R. L. Ralph, and J. B. Adams 1980. Effects of overlapping optical absorption band of pyroxene and glass on the reflectance spectra of lunar soils. *Proc. Lunar Planet. Sci. Conf. 11th,* 719–729.

Feierberg, M., L. Lebofsky, and D. Tholen 1985. The nature of C-class asteroids from 3-μm spectrophotometry. *Icarus* **63,** 183–191.

Gaffey, M. J. 1984. Rotational spectral variations of asteroid 8 Flora: Implications for the nature of the S-type asteroids and for the parent bodies of the ordinary chondrites. *Icarus* **60,** 83–114.

Gaffey, M. J., and S. J. Ostro 1987. Surface lithologic heterogeneity and body shape for asteroid (15) Eunomia: Evidence from rotational spectral variations and multi-color lightcurve inversions. *Lunar Planet. Sci. XVII,* 310–311.

Gaffey, M. J., J. F. Bell, R. H. Brown, and T. Burbine 1990. Mineralogical variations within the S-asteroid population. *Lunar Planet. Sci. XXI,* 399–400.

Gaffey, M. J., J. F. Bell, R. H. Brown, T. H. Burbine, J. L. Piatek, K. L. Reed, and D. A. Chaky 1993a. Mineralogical variations within the S-type asteroid class. *Icarus* **106,** 573–602.

Gaffey, M. J., J. F. Bell, R. H. Brown, T. H. Burbine, J. L. Piatek, K. L. Reed, and D. A. Chaky 1993b. Spectral evidence of size dependent space weathering processes on asteroid surfaces. *Lunar Planet. Sci. XXIV,* 515–516.

Hapke, B. 1993. Why is the Moon dark? *Lunar Planet. Sci. XXIV,* 605–606.

Helfenstein, P., J. Veverka, P. Thomas, T. V. Johnson, A. McEwen, J. Granahan, F. Fanale, P. Geissler, M. Belton, C. Chapman, and the Galileo Imaging Team 1994. Regolith and composition of Ida: Clues from color and photometry. *Bull. Am. Astron. Soc.* **26**(3), 1158.

Hiroi, T., M. E. Zolensky, and M. E. Lipshutz 1995. Mineralogy and spectroscopy of heated Allende meteorite and a K-type asteroid 221 EOS. *19th NIPR Symp. Antarct. Meteorites,* June 6–8, 1995.

Hiroi, T., J. F. Bell, H. Takeda, and C. M. Pieters 1993a. Modeling of S-type asteroid spectra using primitive achondrites and iron meteorites. *Icarus* **102,** 107–116.

Hiroi, T., C. M. Pieters, M. E. Zolensky, and M. E. Lipshutz 1993b. Evidence of thermal metamorphism on C, G, B, and F asteroids. *Science* **261,** 1016–1018.

Hörz, F., and R. B. Schaal 1981. Asteroidal agglutinate formation and implications for asteroidal surfaces. *Icarus* **46,** 337–353.

Johnson T. V., and F. P. Fanale 1973. Optical properties of carbonaceous chondrites and their relationship to asteroids. *J. Geophys. Res.* **78,** 8507–8518.

Keil, K., J. F. Bell, and D. T. Britt 1992. Reflection spectra of shocked ordinary chondrites and their relationship to asteroids. *Icarus* **98,** 43–53.

Keller, L. P., and D. S. McKay 1992. Impact glasses and vapor condensates in Apollo 11 soil. *Lunar Planet. Sci. XXIII,* 673–674.

McFadden, L. A. 1983. S-type asteroids and their relation to ordinary chondrites. *Meteoritics* **18,** 352.

McKay, D. S., T. D. Swindle, and R. Greenberg 1989. Asteroidal regoliths: What we do not know. In *Asteroids II* (R. P. Binzel, T. Gehrels, and M. S. Matthews, Eds.), pp. 98–127. Univ. of Arizona Press, Tucson.

McSween, H. Y., Jr. 1992. Redox effects in ordinary chondrites and implications for asteroid spectrophotometry. *Icarus* **95,** 239–243.

McSween, H. Y., Jr., M. E. Bennett, and E. Jarosewich 1991. The mineralogy of ordinary chondrites and implications for asteroid spectrophotometry. *Icarus* **90,** 107–116.

Moroz, L. V., and C. M. Pieters 1991. Reflectance spectra of some fractions of Migei and Murchison CM chondrites in the range of 0.3–2.6 microns. *Lunar Planet. Sci. XXII,* 923–924.

Nash, D. B., and J. E. Conel 1973. Vitrification darkening of rock powders: Implications for optical properties of the lunar surface. *Moon* **8,** 346–364.

Pieters, C. M. 1984. Asteroid-meteorite connection: regolith effects implied by lunar reflectance spectra. *Meteoritics* **19,** 290–291.

Pieters, C. M., E. M. Fischer, O. Rode, and A. Basu 1993. Optical effects of space weathering: The role of the finest fraction. *J. Geophys. Res. Planets* **98,** 20817–20824.

Salisbury, J. W. 1993. Mid-infrared spectroscopy: laboratory data. In *Remote Geochemical Analysis: Elemental and Mineralogical Composition* (C. M. Pieters and P. A. J. Englert, Eds.), pp. 79–98. Cambridge Univ. Press, New York.

Shkuratov, Yu. G. 1994. Light-backscattering studies of atmosphereless celestial bodies. Measurements of the negative polarization. *Astron. Vestn.* **28**(3), 23–29. [Russian]

Starukhina, L. V., Yu. G. Shkuratov, O. D. Rode, and C. M. Pieters 1994. Reflectance spectra of particle size separates of lunar soils: Is the difference controlled by reduced iron? *Lunar Planet. Sci. XXV,* 1333–1334.

Sunshine, J. M., C. M. Pieters, and S. F. Pratt 1990. Deconvolution of mineral absorption bands: an improved approach. *J. Geophys. Res.* **95,** 6955–6966.

Tedesko, E. F. 1989. Asteroid magnitudes, UBV colors, and IRAS albedos and diameters. In *Asteroids II* (R. P. Binzel, T. Gehrels, and M. S. Matthews, Eds.), pp. 1091–1138. Univ. of Arizona Press, Tucson.

Tholen, D. J. 1984. *Asteroid Taxonomy from Cluster Analysis of Photometry.* Ph.D. thesis, University of Arizona, Tucson.

Vilas, F., and B. A. Smith 1985. Reflectance spectrophotometry (~0.5–1.0 μm) of outer-belt asteroids: Implications for primitive organic solar system material. *Icarus* **64,** 503–513.

Weidner, V. R., and J. J. HSIA 1981. Reflection properties of pressed polytetraflourethylene powder. *J. Opt. Soc. Am.* **71,** 856–860.

Yakovlev, O. I., Yu. P. Dikov, and M. V. Gerasimov 1992. Redox processes during shock events. *Geokhimia* **12,** 1359–1370. [Russian]

Zellner, B., D. J. Tholen, and E. F. Tedesco 1985. The eight-color asteroid survey: Results for 589 minor planets. *Icarus* **61,** 355–416.

Zinovieva, N. G., O. B. Mitreikina, and L. B. Granovsky 1994. Crystallization in the silicate part of the experimental melted ordinary chondrite Tsarev (L5). *Lunar Planet. Sci. XXIV,* 1559–1560.